Dynamic Resonance Analysis and Oscillation Damping of Multi-Terminal DC Grids

Yuchao Liu, Ali Raza, Kumars Rouzbehi, *Senior Member*, *IEEE*, Binbin Li, *Member*, *IEEE*, Dianguo Xu, *Fellow, IEEE*, and B.W. Walliams

***Abstract*—Voltage source converter (VSC) based multi-terminal high voltage direct current (VSC-MTDC) systems/grids are prone to system instability. This critical issue is overlooked in literature. In order to improve the system stability, this paper proposes an effective active damping method as a remedy to suppress voltage and power resonances in the VSC-MTDC grids by injecting damping signals into the inner current loops of VSC-MTDC stations. With dynamic regulation of the damping current, resonance is suppressed by power converter controllers without any additional current and voltage measurement. In this study, modeling and stability analysis of VSC-MTDC system/grid is presented considering the dc-side energy storage components, and control with a droop control structure. Then, single-frequency and multi-frequency resonance mechanisms of dc-bus voltage and power in the event of transients are analyzed. Later, stability effect of MTDC system/grid inductance and capacitance values to the resonance amplitude and frequency droop coefficients is investigated. A PSCAD/EMTDC platform is developed to conduct dynamic simulations, and a scaled-down four-terminal 20 kW experimental prototype is used to validate the effectiveness of proposed control methodology.**

***Index Terms*—Multi-Terminal, VSC-HVDC, dc-LC filter, resonance suppression, active damping**

I. Introduction

THE development and application of renewable energy sources has led to a worldwide proliferation of high voltage direct current (HVDC) projects [1], [2]. The evolution of voltage source converter (VSC) based multi-terminal HVDC (VSC-MTDC) systems is started from the point-to-point VSC-HVDC transmission systems. MTDC systems are promising technology for integrating offshore wind farms (OWF) with mainland grids, for long distance bulk power delivery, city infeed, and construction of future super grids. It offers several advantageous features such as black-start capability, connecting weak ac-grids, and bidirectional power flow [3]-[5]. In recent years, the VSC-MTDC grids have received a great attention from academia and industry pioneers in order to minimize the integration challenges of distributed generation. Compared with the traditional point-to-point VSC based direct current transmission systems, VSC-MTDC has advantages of higher reliability, more robustness, better self-protection performance and more flexibility. Particularly, it is suited to realize the interconnection of offshore wind farms [6], [7]. However, VSC-MTDC system dynamics directly influence the system stability and dynamic performance, therefore an extensive research on this topic is necessary.

In a MTDC grid, a critical parameter of VSC stations connected to MTDC network is the value of dc-bus capacitance. It is designed by taking into account the voltage ripple and controller dynamics [8], [9]. Although there are improvements in MMC based converters which eliminate the need to connect large dc-bus capacitor in the dc grid but the problem of the highly inductive dc grid is still a concern regarding dc circuit breakers (DCCB) and lengthy dc lines. A dc reactor is usually connected on the dc side of VSC stations to suppress the dc fault current peak, and to reduce the current rising rate and the transients in the dc overvoltage [10], [11]. The dc inductance is determined by the turn-off time of DCCB and its maximum current blocking ability, which is limited to its cost [12], [13]. The dc inductance leads to additional transmission losses, cost effectiveness and affects the system stability. Furthermore, the increase of dc inductance effectively slowing down the propagation of dynamic change of dc currents from one terminal to another [14]. The dc capacitor and inductor connected in the dc grid and the inductance and capacitance existed in the dc lines form a dc-LC filter. It directly affects the dynamic response of the dc-link voltage and the instantaneous power in the MTDC system, especially when the dc transmission lines are long enough. Thus, the role of inductance and capacitance in the MTDC grid cannot be ignored [15].

This work was supported in part by the National Natural Science Foundation of China (Grant No. 51237002) and the National High Technology Research and Development Program 863 of China (2015AA050603).

Y. Liu, B. Li and D. Xu are with the Department of Electrical Engineering, Harbin Institute of Technology, Harbin, China.

A. Raza is with the Department of Electrical Engineering, The University of Lahore, Lahore, Pakistan.

K. Rouzbehi is with the Loyola University Andalucia, Seville, Spain, Spain.

B. W. Walliams is with the Strathclyde University, Glasgow, UK.

Numerous studies have been conducted on the dynamic control of VSC-MTDC, where transients of dc-link voltage and power oscillations are addressed in [16]-[20]. Direct voltage fluctuations caused by dynamic change in the dc grid are discussed in [16]. The dynamics and robust control of a MTDC system considering the instantaneous power of both the ac and dc side energy storage components is presented in [17]. However, the transients of dc-link voltage and power oscillations are neglected. A VSC-MTDC model is derived mathematically in [18], and dc voltage control and power sharing in a MTDC system based on droop control, is proposed in [19]. However, the shortcoming is the voltage and current oscillations that have not been suppressed. Oscillation damping techniques have been considered in [16], [21]-[23]. In [16], Guo Li et al. proposed an active damping method based on a low-pass filter, but the filter bandwidth is difficult to select. Inter area oscillation damping scheme using active-power modulation of MTDC grid is presented in [21], but the pairing of two terminals in the MTDC system is difficult to establish. Suppression of the dc voltage fluctuations caused by fast transient power changes is achieved in [22]-[23]. However, it is difficult to precisely damp the fluctuations when considering the power loop bandwidth. Thus, a voltage feed-forward controller is introduced in the droop controller, and the voltage deviation signal after a band pass filter is added to the reference signal of the inner current controller to eliminate the voltage fluctuations. At present, the stability of MTDC grid has attracted great concern. To the best of authors' knowledge, the dynamics and control of MTDC systems with damping for voltage and power oscillation caused by the dynamic change in the system have not been presented in the literature.

In order to solve the mentioned shortcomings, this paper analyses the energy storage components of the MTDC grid and the effect of droop coefficients on the low-frequency dc-link voltage oscillations, which causes power oscillations. To address this issue, an active damping method which modifies the current reference in *dq* reference frame is proposed.

The rest of the paper is organized as follows: section II deals with modeling, analysis and transfer functions of VSC based MTDC system. In Section III, the dc-link voltage resonance principle and effect of dc-link impedance parameters on the system stability is analyzed. Proposed resonance active damping method for VSC-MTDC systems is explained in section IV. Proposed control method is validated though simulation and experimental results in section V. Finally, conclusions are drawn.

II. Modeling of MTDC Grid

This study considers a four-terminal MTDC grid as shown in Fig.1. For notation brevity, subscript *i* represents the i^{th} VSC (VSC*i*, *i* =1, 2,...) and, U_{dci}, i_{dci}, P_i, Q_i represent the direct voltage, direct current, active and reactive powers, respectively. The power direction from the ac to dc side is defined as positive.

To consider the effect of dc lines on low-frequency oscillations, the modelling of dc lines has great importance. Typically, single π section equivalent circuit [24], multiple π sections equivalent circuit [25], and the frequency-dependent [26] cable models are used for studies on stability analysis. In the equivalent MTDC grid, the equivalent impedance of dc lines is modeled as multiple cascaded π sections which are represented by a simple series *R-L* circuit, and a shunt capacitor *C*. For large values of MTDC grid capacitances, the influence of a single π section and multiple cascaded π sections are similar [27]. And the single π section model is sufficiently accurate up to 100 Hz [14]. This paper focuses on the low-frequency resonance which is less than 50 Hz. Thus in this paper, each dc line is a single π section model to represent the equivalent impedance. Therefore, VSC-MTDC grid is equivalent to the circuit as shown in Fig.2. Here, R_i, L_i, and C_i are the equivalent dc resistance, inductance and dc capacitance of i^{th} VSC. R_{ij}, L_{ij}, and C_{ij} represent the resistance, inductance and capacitance of dc lines between VSC*i* and VSC*j*, respectively. U_{ci} is the dc bus voltage. In order to mitigate the system resonances, damping control is needed within the system controller to stabilize the dc-link voltage and maintain the system control performance, whilst the dc bus capacitor is minimized.

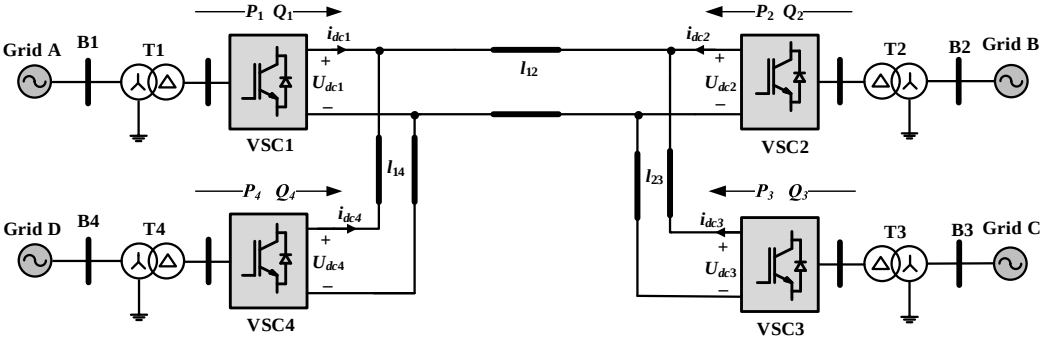

Fig.1 The equivalent diagram of the test MTDC grid

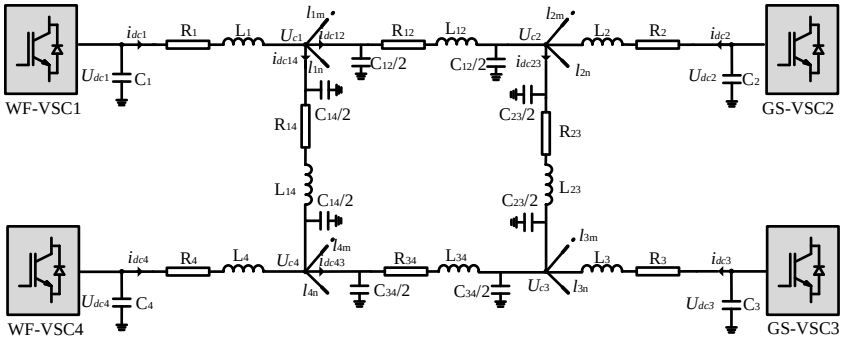

Fig.2 Equivalent dc circuit of the MTDC grid test system

III. Resonance Analysis of MTDC Grid

A. Voltage Droop Control in MTDC Grid

Among the control strategies of VSC-MTDC grids, the voltage-droop control is widely applied because it allows multiple VSC stations to participate in dc voltage control and power sharing simultaneously. The droop coefficients are defined in (1) and (2). From (1), the droop coefficient k_i is equivalent to the multiplicative inverse of damping resistance R_{kd} in the VSC-MTDC grid. So, the value of the droop coefficient has considerable effect on attenuation of voltage oscillation. A larger damping resistance, means a smaller droop coefficient, quickly damps the direct voltage oscillation but causes a large dc voltage deviation during transient states [6].

$$k_i = \Delta P_i / \Delta U_{dci} \tag{1}$$

$$R_{kd} = 1/k_i = \Delta U_{dci} / \Delta P_i \tag{2}$$

Clearly, droop control increases the output resistance of each source, which makes them far from an ideal source. Consequently, the VSC stations with droop control can be equivalent to a controlled current source i_s. The control block diagram of the droop control is shown in Fig.3, where the inner current loop is considered to have perfect closed loop dynamics and is approximated by a first order system with time constant T_s. Thus, the transfer functions G_{d1} and G_{d2} from direct voltage U_{dci} to input current i_s and direct reference voltage U_{dciref} are given in (3) and (4), respectively. The direct voltage can be expressed by the reference direct voltage U_{dciref} and input current i_s as in (5), where C_{eqi}, C_{eqj} is the equivalent capacitance of VSC*i* and VSC*j*. i_L is the inductance current.

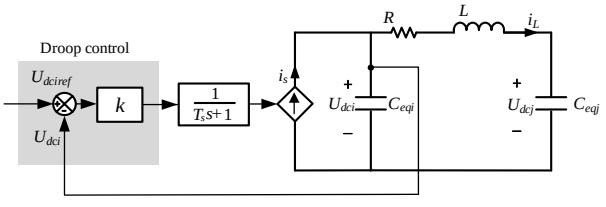

Fig.3 Block diagram of dc-link voltage regulation by voltage-droop control

$$G_{d1} = \frac{U_{dci}}{i_s} = \frac{T_s s + 1}{T_s C_{eqi} s^2 + C_{eqi} s + k_i} \tag{3}$$

$$G_{d2} = \frac{U_{dci}}{U_{dciref}} = \frac{k_i}{T_s C_{eqi} s^2 + C_{eqi} s + k_i} \tag{4}$$

$$U_{dci} = G_{d1} i_s + G_{d2} U_{dciref} \tag{5}$$

B. Analysis of Single-Frequency Resonance MTDC Grid

As mentioned before, each VSC station is considered equivalent to a controlled current source i_s with output current i_{out} and the dc line is modelled as a π section. The π section model of the dc line is introduced in [28]. The equivalent four-terminal MTDC grid with a single π section, is shown in Fig.4. The existing dc line capacitances are added to the dc bus capacitor to give the equivalent capacitors C_{eq1} and C_{eq2}. L and R are the inductance and the resistance in the dc line. Using electrical circuit theory, the system state equations are as follows:

$$i_c + i_{dc} = C_{eq}(dU_{dci}/dt) + i_{dc} = i_s \tag{6}$$

$$u_R + u_L + U_{dcj} - U_{dci} = 0 \tag{7}$$

$$L(di_{dc}/dt) + Ri_{dc} + U_{dcj} - U_{dci} = 0 \tag{8}$$

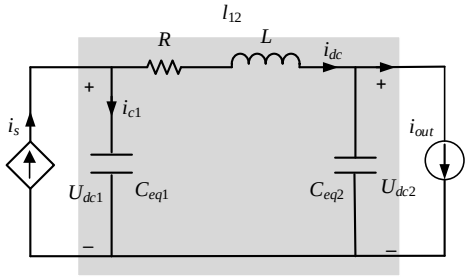

Fig.4 Equivalent circuit of MTDC system with single dc line

The transfer function in frequency domain, after Laplace transform of (8) is (9) that give the relation between the dc current i_{dc} and ac current i_s as in (10):

$$sLi_{dc} + Ri_{dc} + \frac{2i_{dc}}{sC_{eq}} = \frac{i_s}{sC_{eq}} \tag{9}$$

$$\frac{i_{dc}}{i_s} = \frac{1}{sC_{eq}(sL + R + 2/sC_{eq})} \tag{10}$$

Similarly, transfer functions of output direct voltage U_{dci} to input current i_s are as in (11) and (12) for i^{th} and j^{th} VSCs, respectively.

$$G_i = \frac{U_{dci}}{i_s} = \frac{LC_{eq}s^2 + RC_{eq}s + 1}{s(LC_{eq}^2 s^2 + RC_{eq}^2 s + 2C_{eq})} \tag{11}$$

$$G_j = \frac{U_{dcj}}{i_s} = \frac{1}{s(LC_{eq}^2 s^2 + RC_{eq}^2 s + 2C_{eq})} \tag{12}$$

The derivation of (8) is:

$$L\frac{di_{dc}^2}{dt^2} + R\frac{di_{dc}}{dt} + \frac{dU_{dcj}}{dt} - \frac{dU_{dci}}{dt} = 0 \tag{13}$$

Since $C_{eq}(dU_{dcj}/dt) = i_{dc}$, (13) can be simplified to:

$$\frac{di_{dc}^2}{dt^2} + \frac{R}{L}\frac{di_{dc}}{dt} + \frac{2i_{dc}}{LC_{eq}} = \frac{i_s}{LC_{eq}} \tag{14}$$

From (14) following can be deduced:

1) When the dc equivalent capacitance $C_{eq} \geq 8L/R$, the system is stable.
2) When the dc equivalent capacitance $C_{eq} < 8L/R$, the system presents resonance during a transient state.

TABLE I
THE PARAMETERS OF DC LINES

Name	l_{12}	l_{23}	l_{14}
Length of dc line (km)	125	160	80
Resistance (Ω)	1.1875	1.52	0.76
Inductance (H)	0.264	0.338	0.169
Capacitance (μF)	6.25	8	4

DC transmission line parameters are given in Table I. Bode plots of the system with different parameters for single π section is shown in Fig.5(a). As MTDC grid inductance increases, the resonance frequency decreases and the resonance amplitude increases.

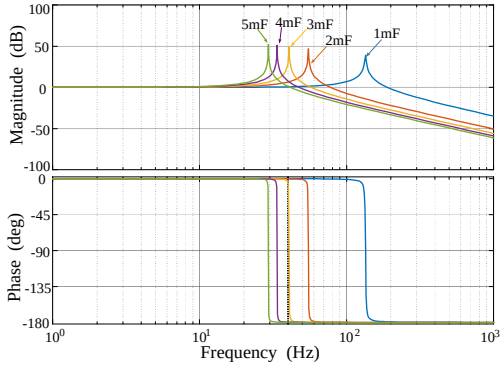

(a) under single dc line

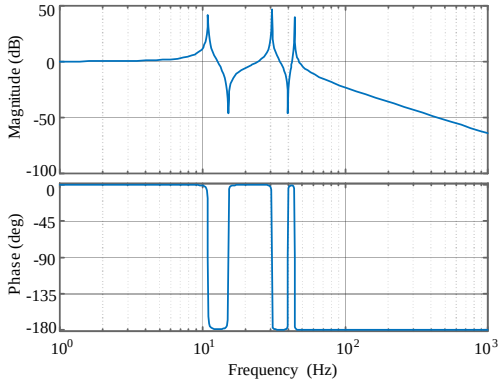

(b) under three dc lines

Fig.5 Bode plots of the MTDC grid with different parameters

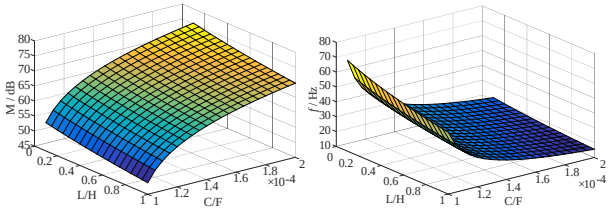

Fig.6 Relationship between (a) resonance magnitude, inductance and capacitance, (b) resonance frequency, inductance and capacitance

C. Analysis of Multi-Frequency Resonance MTDC Grid

In this section, multi-frequency resonance (multiple dc lines) in the MTDC system is analysed. The equivalent circuit of the parallel four-terminal MTDC grid with three dc lines l_{12}, l_{14} and l_{23} is shown in Fig.7, where R_{ij}, L_{ij}, C_{ij} (i=1,2,3…, j=1,2,3…) are the line resistance, line inductance, and the line capacitance between VSCi and VSCj. The test system state equations are:

$$\begin{cases} C_1\dfrac{dU_{dc1}}{dt} = i_{L1} - i_{L2} \\ C_2\dfrac{dU_{dc2}}{dt} = i_{L2} - i_{L3} \\ C_3\dfrac{dU_{dc3}}{dt} = i_{L3} - i_{out} \\ C_4\dfrac{dU_{dc4}}{dt} = i_{s4} - i_{L1} \\ R_1 i_{L1} + L_1\dfrac{di_{L1}}{dt} = U_{dc4} - U_{dc1} \\ R_2 i_{L2} + L_2\dfrac{di_{L2}}{dt} = U_{dc1} - U_{dc2} \\ R_3 i_{L3} + L_3\dfrac{di_{L3}}{dt} = U_{dc2} - U_{dc3} \end{cases} \tag{15}$$

$$\begin{cases} \dot{x} = \mathbf{A}x + \mathbf{B}u \\ y = \mathbf{C}x + \mathbf{D}u \end{cases} \tag{16}$$

$$\mathbf{A} = \begin{bmatrix} 0 & 0 & 0 & 0 & 1/C_1 & -1/C_1 & 0 \\ 0 & 0 & 0 & 0 & 0 & 1/C_2 & -1/C_2 \\ 0 & 0 & 0 & 0 & 0 & 0 & 1/C_3 \\ 0 & 0 & 0 & 0 & -1/C_4 & 0 & 0 \\ -1/L_1 & 0 & 0 & 1/L_1 & -R_1/L_1 & 0 & 0 \\ 1/L_2 & -1/L_2 & 0 & 0 & 0 & -R_2/L_2 & 0 \\ 0 & 1/L_3 & -1/L_3 & 0 & 0 & 0 & -R_3/L_3 \end{bmatrix}$$

$$\mathbf{B} = \begin{bmatrix} 0 & 0 & 0 & 1/C_4 & 0 & 0 & 0 \\ 0 & 0 & -1/C_3 & 0 & 0 & 0 & 0 \end{bmatrix}^{\mathrm{T}}$$

$$\mathbf{C} = \begin{bmatrix} 1 & 0 & 0 & 0 & 0 & 0 & 0 \\ 0 & 1 & 0 & 0 & 0 & 0 & 0 \\ 0 & 0 & 1 & 0 & 0 & 0 & 0 \\ 0 & 0 & 0 & 1 & 0 & 0 & 0 \end{bmatrix}, \quad \mathbf{D}=0$$

where x=[U_{dc1} U_{dc2} U_{dc3} U_{dc4} i_{L1} i_{L2} i_{L3}]$^{\mathrm{T}}$, u=[i_{s4}, i_{out}], and y=[U_{dc1} U_{dc2} U_{dc3} U_{dc4}] $^{\mathrm{T}}$. The state matrices A,

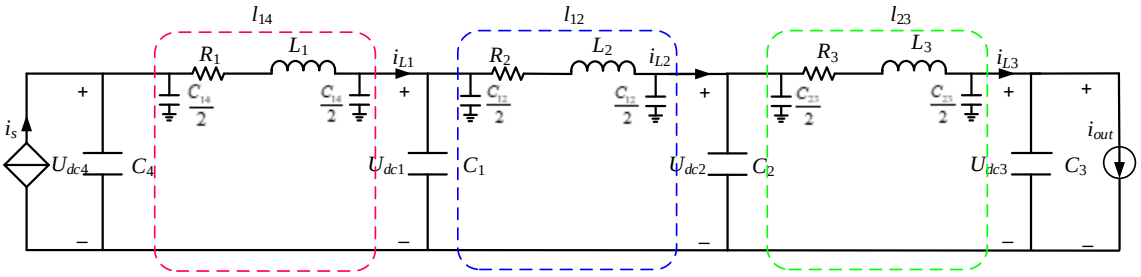

Fig.7 Equivalent circuit of four-terminal MTDC grid with three dc lines

B, C and D are derived from (15). The Bode plots of the transfer function from U_{dc3} to U_{dc4} are illustrated in Fig. 5(b). The MTDC grid with three dc lines generates direct voltage link resonance at three frequencies. Fig.6 is presenting two relationships: (a) between resonant amplitude and frequency (b) system dc impedance and capacitance. In order to suppress the resonance, the dc bus capacitance should be increased because the dc line impedance parameters are determined with its own properties. However, increasing capacitance will increase system volume and costs, which may not be practically acceptable. Consequently, a control method should be used to suppress the resonance.

IV. Active Damping Method for Resonance Suppression

A. Comparison of damping methods for resonance suppression

Typically, resonance damping approaches are classified into passive and active methods. In general with passive damping, a resistor R_d is inserted in series with the capacitor or in parallel with the inductor as illustrated in Fig.8. Derived circuit equations are given in (17), and the state matrices are (18) and (19).

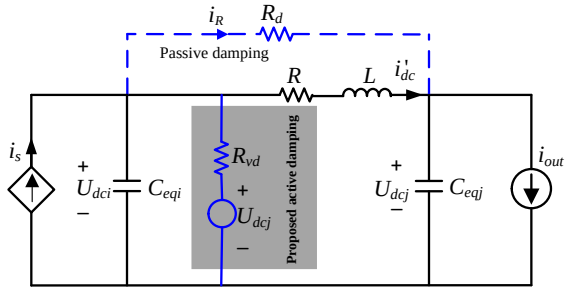

Fig.8 Equivalent circuit of MTDC with damping control.

$$\begin{cases} C_{eqi}\dfrac{dU_{dci}}{dt}+i'_{dc}+\dfrac{U_{dci}-U_{dcj}}{R_d}=i_s \\ C_{eqj}\dfrac{dU_{dcj}}{dt}-i'_{dc}-\dfrac{U_{dci}-U_{dcj}}{R_d}=i_{out} \\ \dfrac{di'_{dc}}{dt}=-\dfrac{R}{L}i'_{dc}-\dfrac{U_{dci}}{L}-\dfrac{U_{dcj}}{L} \end{cases} \tag{17}$$

$$\mathbf{A}_1=\begin{bmatrix} -1/(R_dC_{eqi}) & 1/(R_dC_{eqi}) & -1/C_{eqi} \\ 1/(R_dC_{eqj}) & -1/(R_dC_{eqj}) & 1/C_{eqj} \\ 1/L & -1/L & -R/L \end{bmatrix} \tag{18}$$

$$\mathbf{B}_1=\begin{bmatrix} 1/C_{eqi} & 0 \\ 0 & -1/C_{eqj} \\ 0 & 0 \end{bmatrix} \quad \mathbf{C}_1=\begin{bmatrix} 1 & 0 & 0 \\ 0 & 1 & 0 \\ 0 & 0 & 1 \end{bmatrix} \tag{19}$$

Changing the equivalent impedance of the network by means of a passive component is not a reliable solution. Although passive damping can suppress the resonances, it may also lead to resonances in other frequencies. In addition, with passive damping, current flowing through the parallel resistor introduces extra power losses. Moreover, in the MTDC grid, shunt connected resistor to the dc lines may not be realistic because of its high cost and losses, as the current i_R through the resistor R_d is large. It also attenuates the high-frequency, thereby generating more system harmonics [23]. In order to address these shortcomings, the passive damping method is replaced with an active damping method, which suppresses any oscillation effectively by a control algorithm, without a physical resistor.

An active damping method, equivalent to a passive approach, is depicted in Fig.8, where R_{vd} is the virtual damping resistor. The virtual active damping has the same resonance suppression effect as the passive damping with extra benefit of no power loss because it does not require a physical resistor in the circuit. A new state matrix A_2 under proposed damping method is established in (20) by using the same variables as the passive damping method.

$$\mathbf{A}_2=\begin{bmatrix} -1/(R_dC_{eqi}) & 1/(R_dC_{eqi}) & -1/C_{eqi} \\ 0 & 0 & 1/C_{eqj} \\ 1/L & -1/L & -R/L \end{bmatrix} \tag{20}$$

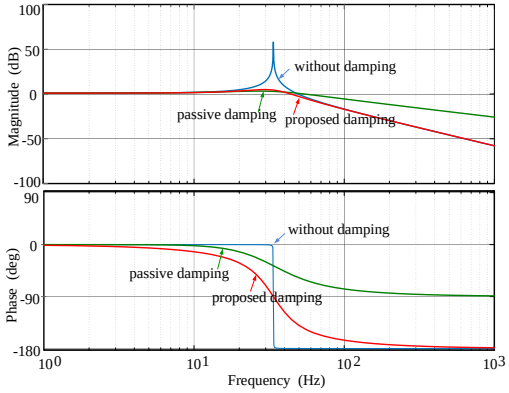

(a) under single-frequency

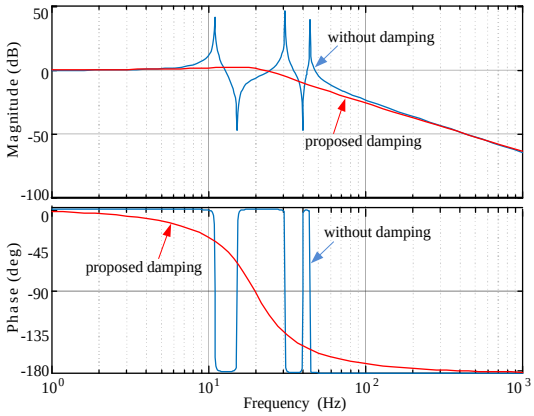

(b) under multi-frequency

Fig.9 Bode plots of the proposed damping methods

The Bode plots of the single-frequency and multi-frequency resonance with passive damping, proposed damping method and without any damping method are depicted in Fig.9(a) and (b) respectively, for the cause of comparison. Plots show that the proposed active damping method works at the resonant frequency. However, the magnitude at high frequency is same as without damping control which means, under the proposed damping control, not only suitable damping performance can be realized but also no high harmonic components are generated.

B. Realization of the Proposed Resonance Suppression Strategy

The fundamental control diagram of VSC-HVDC station comprised of the outer controller and the inner controller as shown in Fig.10**,** where the i_{sa}, i_{sb}, i_{sc}, u_{sa}, u_{sb}, u_{sc}, u_{aref}, u_{bref}, and u_{cref} are the three phases ac current, ac voltage and modulating signals, respectively. PLL is the phase-locked loop. The controller is decoupled in *dq* control, where the *d*-axis controls the direct voltage or active power and *q*-axis regulates the reactive power or ac voltage. i_{sdref}, i_{sqref}, i_{sd}, i_{sq} are the reference value and measured values of *d*-axis and *q*-axis components, respectively. The *q*-axis control mode is dependent on the value of i_{q_mode} for reactive power control or ac voltage control according to the applications. Where Q_{ref}, Q, U_{acref}, U_{ac} are the reference and measured values of reactive power and ac voltage. The *d*-axis control mode depends on the values of *a* and *b*:

1) If a=k, b=1, where k is the droop coefficient, then the system is with voltage-droop control.
2) If a=1, b=0, the control mode is constant voltage control.
3) If a=0, b=1, the control mode is constant power control.

The outer controller for i^{th} VSC controller based on the proposed damping method is described by:

$$\Delta i_{sdi} = \left(k_{pi} + \frac{k_{si}}{s}\right)\left[(P_{iref} - P_i) + k_i(U_{dciref} - U_{dci})\right] - \left(\frac{U_{dci}}{1.5U_{sdi}}\frac{U_{dci} - U_{dcj}}{R_{vd}} + 1\right)i_{sdi} \qquad i = 1, \cdots, j, \cdots \tag{21}$$

where, k_{pi} and k_{si} are the proportional and integral gains of the droop controller, respectively. P_{iref}, P_i, U_{dciref}, U_{dci} denote the reference and measured values of active power and dc voltage at the i^{th} VSC station, respectively. U_{sdi} and i_{sdi} are the *d*-axis components of three phase ac voltage and ac current while k_i is the droop coefficient of the i^{th} converter.

In order to realize the proposed resonance suppression strategy, the VSC controller is modified. The virtual direct current signal i_{vd} is transformed to ac signal and added to the modulation signals. The current through the virtual resistor i_{vd} of Fig.8 is given in (22). Ignoring the power converter losses, the ac power is equal to the dc power. The relationship between virtual current i_{vd} and the d-axis component i_{sd} of ac current in the *dq* frame can be obtained from (23) and (24). Hence, the virtual current i_{vd} is added to the inner loop controller of the power converter. The modified control block diagram is shown in Fig.10. The proposed method is advantageous as it requires no additional sensors and is easy to implement. Such a method finds its applications in MTDC grid where VSC stations are at risk of dynamic change.

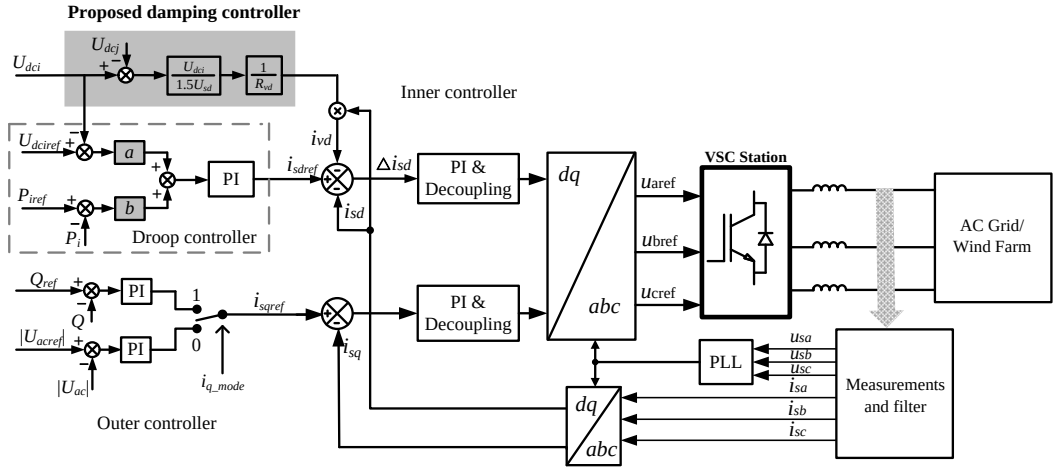

Fig.10 The proposed control diagram of VSC station with resonance suppression strategy

$$i_{vd} = \frac{U_{dci} - U_{dcj}}{R_{vd}} \tag{22}$$

$$P = U_{dc} i_{dc} = \frac{3}{2} U_{sd} i_{sd} \tag{23}$$

$$i_{vd} = \left(\frac{U_{dci}}{1.5 U_{sdi}} \right) \left(\frac{U_{dci} - U_{dcj}}{R_{vd}} \right) i_{sd} \tag{24}$$

V. Simulation and Experimental Results

In order to verify and validate the effectiveness of the modelling and analysis of the proposed control strategy for VSC-MTDC grids, a four-terminal VSC-MTDC grid of Fig. 1 is simulated and experimentally configured viz., power change and permanent disconnection of a VSC. For observation convenience, the dc-link voltage and power values are presented in per-unit. In this network, converters VSC2 and VSC3 are droop controlled while VSC1 and VSC4 are interfaced with offshore wind farms and power loads, operating with fix power control.

TABLE II
DESIGNED SYSTEM PARAMETERS

Name of parameters	Specifications
Nominal reference direct voltage U_{dcref}/kV	200 (1 pu)
Active power base value /MW	2
Initial active power of VSC1 /MW	2 (1 pu)
Initial active power of VSC2 /MW	-1 (0.5 pu)
Initial active power of VSC3 /MW	-2 (-1 pu)
Initial active power of VSC4 /MW	1 (0.5 pu)
Ratio of the coupling transformer (kV/kV)	380/200
Equivalent resistance in ac side R_i/Ω	1.2
Equivalent inductance in ac side L_i/mH	1.58
DC capacitance C/μF	700
Droop coefficient of VSC2 k_2	10
Droop coefficient of VSC3 k_3	5
Passive damping resistor R_d/Ω	15
Virtual active damping resistor R_{vd}/Ω	15

A. Simulation Results

The configuration of Fig. 1 is assessed with proposed active damping and without any damping technique through simulations developed in PSCAD/EMTDC. DC link and control parameters of Table I and II, respectively, are used to suppress the resonance caused by the system dynamics. Two tests are formulated as described in the subsequent (a) and (b) sub-sections.

(a) At t=1.0 s, power through VSC4 is reversed from 0.5 pu to -0.5 pu as shown in first half of Fig.11. In order to keep the balance of power transmission in the MTDC grid, the dc link voltage is reduced by 0.05 pu. Meanwhile, VSC2 and VSC3 regulate their active power to share the power deviation caused by VSC4. As the power deviation of VSC4 is 1.0 pu, VSC2 and VSC3 reduce power to 0.66 pu and 0.33 pu, respectively. VSC station with a larger droop coefficient shares more power and hence cause larger resonance amplitude. Therefore, resonance amplitude of VSC2 is twice that of VSC3.

(b) At t=2.0 s, VSC1 is permanently disconnected from the system because of a symmetrical ac fault on grid A as shown in second half of Fig.11. Thus, VSC2 and VSC3 collectively compensate the power deviation caused by disconnection of VSC1.

1) *Results without damping*: Fig.11(a), (b), and (c) show the dynamic results without damping for single dc line and multiple dc lines, respectively. The dc-link voltage and power profiles appear as single-frequency resonance with single dc line, and multi-frequency resonance with multiple dc lines, in the transient state. It is clear from Fig.11(a)-(c) that as the inductance increases, the resonance amplitude and frequency reduced which confirms the analysis illustrated in Fig.6. In addition, the harmonic analysis of the active power P_2 under different simulation scenarios are shown in Fig.12(a), (b), and (c). As analysed in section III, the resonance frequencies under different conditions well matched with the analysis of Fig.5 and Fig.6, respectively. Test results verified that the transient dc-link voltage and power resonances are caused by the energy storage components in the MTDC grid. The ability of sharing the power deviation is dependent on the droop coefficients, which are proportional to the power deviation sharing and the resonance amplitude.

2) *Results with proposed active damping:* To mitigate the aforementioned effects, simulations are performed for the designed MTDC grid with the proposed active damping method and multiple π sections dc lines.

The dc-link voltage and power profiles for power variation and permanent VSC disconnection tests are shown in Fig. 11(d). The harmonic analysis of active power P_2 under the proposed active damping method is presented in Fig.12(d). Plots show that the dc-link voltage and power resonance profiles are well suppressed. Suppression of single and multi-frequency resonances are same. That's why results for only multi-frequency are presented here. VSC stations quickly respond to the dynamic change in the system with active damping. All of the dc-link voltages are within the permissible range of ±10%. This avoids overvoltage and overloading of VSC stations during transients as well as improves the stability and robustness of the MTDC grid.

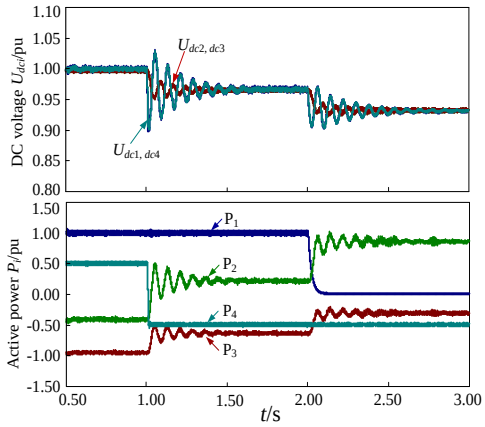

(a) Single dc line without damping (L=0.264H)

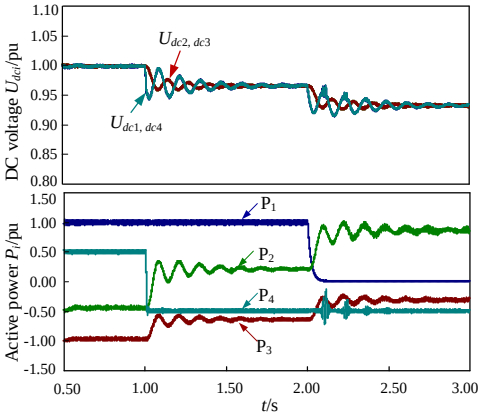

(b) Single dc line without damping (L=0.528H)

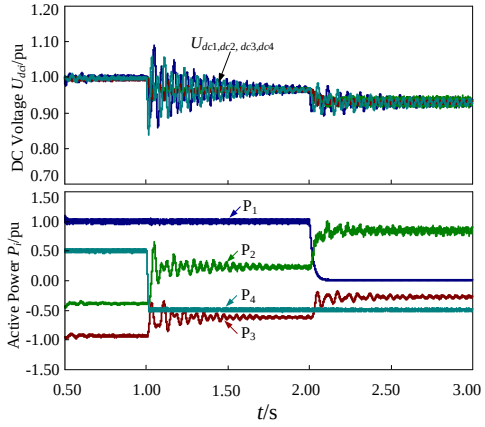

(c) Multiple dc lines without damping

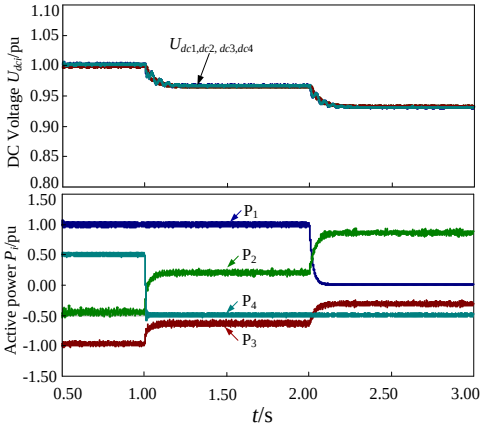

(d) With proposed damping method

Fig.11 Voltage and power profiles of MTDC grid

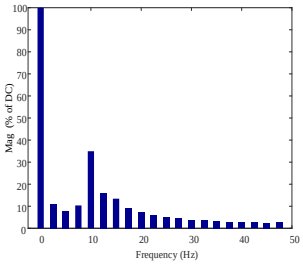

(a) Single dc line without damping L=0.264H

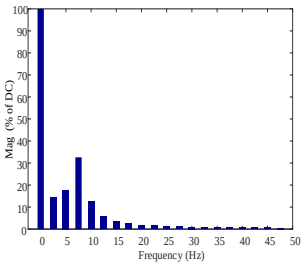

(b) Single dc line without damping L=0.528H

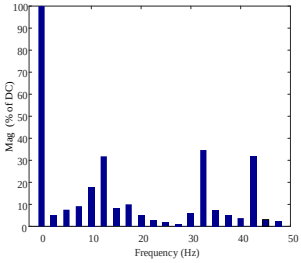

(c) Multiple dc lines without damping

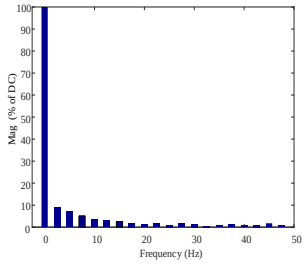

(d) Multiple dc lines with proposed damping method

Fig.12 The Fourier analysis under different scenarios

B. Experimental Results

Configuration of Fig. 1 is assessed to validate the effectiveness of the proposed active damping control strategy and the analysis of the single, and multi-frequency resonances with the experimental platform. A 20 kW four-terminal HVDC grid based on two-level VSC workbench is established in lab as shown in Fig. 13, using the control parameters in Table II. The decentralized voltage droop control is applied to the grid connected VSCs while the WF connected VSCs operate with a fix active power and ac voltage control to extract maximum power. The experiments are performed at a low voltage level because of laboratory experimental setup components restrictions. The dc and ac voltages, and the nominal power of VSCs presented in Table II are scaled-down to 1000:1. So, the experimental results are also attenuated.

The dc lines are modeled using dc resistors, capacitors and inductors in a π section fashion according to Table I. Lengths of dc lines l_{12}, l_{23} and l_{14} are scaled-down to 100:1, which means the length of l_{12}, l_{23} and l_{14} are 1.25 km, 1.6 km and 0.8 km, respectively.

The control strategy and the droop coefficients are same as for the simulations. Validation of the proposed resonance suppression method is experimentally tested through power change and permanent VSC disconnection. Experimental case studies are presented in the following (a) and (b) sub-sections. The measurements are done with Yokogawa DL850E scope coder.

(a) At $t=t_1$, VSC4 power is instantaneously reversed from 0.5 pu to -0.5 pu. The power deviation caused by VSC4 is compensated reasonably by VSC2 and VSC3 with droop control, according to their respective droop coefficients as shown in first half of Fig.14. Resonance amplitude of VSC2 is twice that of VSC3 because of larger droop coefficient of VSC2.

(b) At $t=t_2$, VSC1 is permanently disconnected from dc grid because of the symmetrical ac grid fault on grid A. Power deviation caused by VSC1 disconnection is compensated through VSC2 and VSC3 collectively as shown in second half of Fig.14.

1) *Results without damping*: Dynamic experimental results without passive damping for a dc line and multiple dc lines are shown in Fig.14(a) and (b), respectively, under two conducted tests. Resonance amplitude and frequency is reduced as inductance increased in Fig.14(a) and (b) which

confirms the analysis illustrated in Fig.6. Experimental results proved that the energy storage components in the MTDC grid are the cause of transients of dc-link voltage and resonances in power profile. Moreover, power deviation sharing and the resonance amplitude is droop coefficient's dependant.

2) *Results with proposed active damping:* As with the simulations, the MTDC system experimental results with proposed damping method for multiple dc lines are illustrated in Fig.14(c).

The power deviations caused by VSC4, during test-1, and VSC1, during test-2, respectively, are compensated reasonably by VSC2 and VSC3 with droop control, according to their respective droop coefficients, as illustrated in first and second half of Fig.14(c), respectively. The dc-link voltage and power resonance profiles are well suppressed with the proposed active damping technique. Suppression of single and multi-frequency resonances are same. That's why results for active damping only with multi-frequency are presented. Thus, effectiveness of the proposed damping method to suppress transient resonances caused by energy storage components is validated.

Simulation and experimental results are well matched as clear from Fig.11 and Fig.14. Thus, active damping based control strategy find its applications in MTDC grids where VSC stations are at risk of transients due to power change, load demand change or eventual VSC disconnections. Overall, proposed method is even cheaper and easy to implement than passive damping as it do not require additional sensors.

Fig.13. Experimental platform of four-terminal VSC-HVDC test grid.

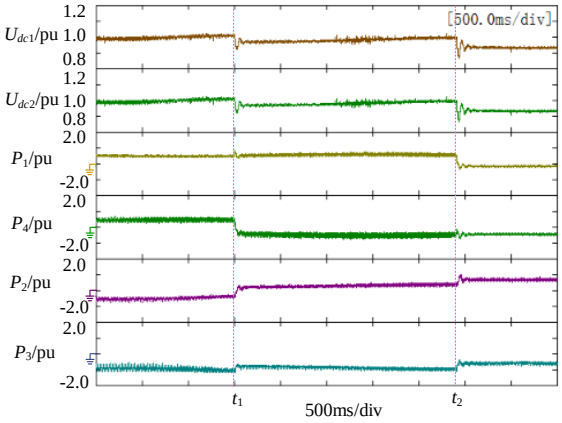

(a) under a single dc line without damping

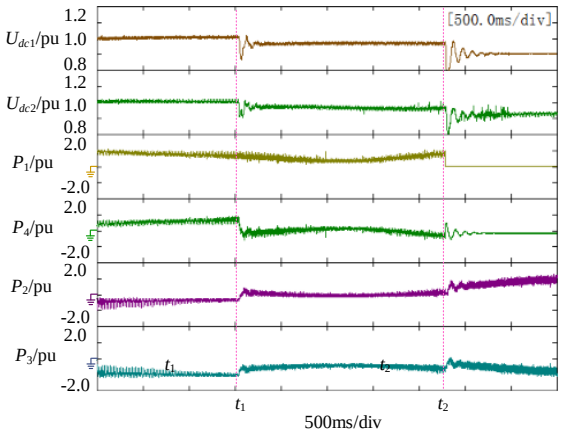

(b) under multiple dc lines without damping

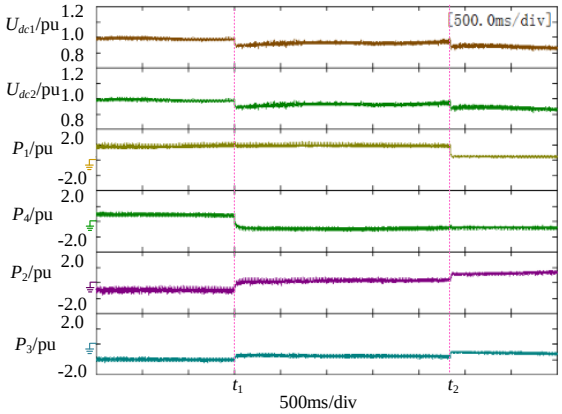

(c) under multiple dc lines with proposed damping method

Fig.14. MTDC grid experimental results

VI. Conclusion

An active damping method has been proposed for VSC-MTDC grid to suppress the direct voltage and power resonances considering the influence of dc grid parameters on VSC-MTDC system's stability. Relationship between dc and ac powers used to develop the proposed technique through modification in the inner current reference. Droop coefficients designed to regulate the dc-link voltage, power and amplitude of resonance as transients mainly caused by the energy storage components. A VSC-MTDC grid was modeled, analyzed and the transfer function between the input current and dc-link voltage was deduced. Relationships between resonant amplitude and frequency, the system impedance and capacitance parameters of MTDC grid were analyzed, respectively.

A four terminal VSC based HVDC scaled down experimental platform and simulations developed in PSCAD/EMTDC were used to assess the effectiveness of the designed active damping strategy to achieve direct voltage and power profiles free from resonances during transients. Several case studies were conducted, including wind power variation and loss of a grid-side VSC. The results showed good system performance, all in accordance with the proposed control scheme specifications during both steady and transient states.

Such a damping method finds its application in MTDC grids where VSC stations are at risk of transients. In addition, the proposed method is cheap and easy to implement than passive damping as it does not require additional sensors.

ACKNOWLEDGMENT

The authors gratefully acknowledge the contributions of the National Natural Science Foundation of China (Grant No. 51237002) and the National High Technology Research and Development Program 863 of China (2015AA050603).

REFERENCES

[1] T. Ackermann, “Transmission systems for offshore wind farms,” *IEEE Power Eng. Rev.*, vol. 22, no. 12, pp. 23–27, Dec. 2002.

[2] P. Bresesti, W. L. Kling, R. L. Hendriks, and R. Vailati, “HVDC connection of offshore wind farms to the transmission system,” *IEEE Trans. Energy Convers.*, vol. 22, no. 1, pp. 37–43, Mar. 2007.

[3] N. Flourentzou, V. G. Agelidis and G. D. Demetriades, "VSC-Based HVDC Power Transmission Systems: An Overview," *IEEE Transactions on Power Electronics*, vol. 24, no. 3, pp. 592-602, March 2009

[4] Z. d. Wang *et al*., "A Coordination Control Strategy of Voltage-Source-Converter-Based MTDC for Offshore Wind Farms," *IEEE Transactions on Industry Applications*, vol. 51, no. 4, pp. 2743-2752, July-Aug. 2015.

[5] M. Davari and Y. A.-R. I. Mohamed, “Robust multi-objective control of VSC-based DC-voltage power port in hybrid AC/DC multi-terminal microgrids,” *IEEE Trans. Smart Grids*, vol. 4, no. 3, pp. 1597–1612, Sep. 2013.

[6] Gavriluta, C., et al., “Design considerations for primary control in multi-terminal VSC-HVDC grids”. *Electric Power Systems Research*, 2015. 122: 33-41.

[7] A. Raza, X. Dianguo, L. Yuchao, S. Xunwen, B. W. Williams and C. Cecati,"Coordinated Operation and Control of VSC Based Multiterminal High Voltage DC Transmission Systems," *IEEE Trans. Sustain. Energy*, vol. 7, no. 1, pp. 364-373, Jan. 2016.

[8] Y. Tang, L. Ran, O. Alatise and P. Mawby, "Capacitor Selection for Modular Multilevel Converter," in *IEEE Transactions on Industry Applications*, vol. 52, no. 4, pp. 3279-3293, July-Aug. 2016.

[9] C. Gavriluta, I. Candela, A. Luna, J. Rocabert and P. Rodr ́guez, "Adaptive droop for primary control in MTDC networks with energy storage," *Power Electronics and Applications (EPE), 2013 15th European Conference on*, Lille, 2013, pp. 1-9.

[10] Wen Jialiang, Wu Rui, Peng Chang, Wang Yu, “Analysis of DC Grid Prospects in China,” *Proceedings of the CSEE*, vol. 32, no. 13, pp. 7-12, 2012.

[11] R. T. Pinto, S. F. Rodrigues, P. Bauer and J. Pierik, "Comparison of direct voltage control methods of multi-terminal DC (MTDC) networks through modular dynamic models," *Power Electronics and Applications (EPE 2011), Proceedings of the 2011-14th European Conference on*, Birmingham, 2011, pp. 1-10.

[12] J. Descloux, B. Raison and J. B. Curis, "Protection algorithm based on differential voltage measurement for MTDC grids," *Developments in Power System Protection (DPSP 2014), 12th IET International Conference on*, Copenhagen, 2014, pp. 1-5.

[13] L. Tang and B. T. Ooi, "Locating and Isolating DC Faults in Multi-Terminal DC Systems," *IEEE Transactions on Power Delivery*, vol. 22, no. 3, pp. 1877-1884, July 2007.

[14] W. Wang, M. Barnes, O. Marjanovic and O. Cwikowski, "Impact of DC Breaker Systems on Multiterminal VSC-HVDC Stability," *IEEE Transactions on Power Delivery*, vol. 31, no. 2, pp. 769-779, April 2016.

[15] C. M. Franck, "HVDC Circuit Breakers: A Review Identifying Future Research Needs," *IEEE Transactions on Power Delivery*, vol. 26, no. 2, pp. 998-1007, April 2011.

[16] Guo Li, Feng Zebin, Li Xialin, et al. “Stability Analysis and Research of Active Damping Method for DC Microgrids,” *Proceeding of CSEE*, vol 36, no. 4, pp. 927-936, 2016.

[17] M. Davari and Y. A. R. I. Mohamed, "Dynamics and Robust Control of a Grid-Connected VSC in Multiterminal DC Grids Considering the Instantaneous Power of DC- and AC-Side Filters and DC Grid Uncertainty," *IEEE Transactions on Power Electronics*, vol. 31, no. 3, pp. 1942-1958, March 2016.S. Cole,

[18] J. Beerten and R. Belmans, "Generalized Dynamic VSC MTDC Model for Power System Stability Studies," *IEEE Transactions on Power Systems*, vol. 25, no. 3, pp. 1655-1662, Aug. 2010.

[19] K. Rouzbehi, A. Miranian, A. Luna and P. Rodriguez, "DC Voltage Control and Power Sharing in Multiterminal DC Grids Based on Optimal DC Power Flow and Voltage-Droop Strategy," *IEEE Journal of Emerging and Selected Topics in Power Electronics*, vol. 2, no. 4, pp. 1171-1180, Dec. 2014

[20] E. Prieto-Araujo, A. Egea-Alvarez, S. Fekriasl and O. Gomis-Bellmunt, "DC Voltage Droop Control Design for Multiterminal HVDC Systems Considering AC and DC Grid Dynamics," *IEEE Transactions on Power Delivery*, vol. 31, no. 2, pp. 575-585, April 2016.

[21] L. Harnefors, N. Johansson, L. Zhang and B. Berggren, "Interarea Oscillation Damping Using Active-Power Modulation of Multiterminal HVDC Transmissions," *IEEE Transactions on Power Systems*, vol. 29, no. 5, pp. 2529-2538, Sept. 2014.

[22] K. Rouzbehi, J. I. Candela, A. Luna, G. B. Gharehpetian and P. Rodriguez, "Flexible Control of Power Flow in Multiterminal DC Grids Using DC–DC Converter," *IEEE Journal of Emerging and Selected Topics in Power Electronics*, vol. 4, no. 3, pp. 1135-1144, Sept. 2016.

[23] J. Lei, B. Zhou, X. Qin, J. Wei and J. Bian, "Active damping control strategy of matrix converter via modifying input reference currents," *IEEE Transactions on Power Electronics*, vol. 30, no. 9, pp. 5260-5271, Sept. 2015.

[24] Prieto-Araujo, E., Bianchi, F.D., Junyent-Ferre, A., et al.: ‘Methodology for droop control dynamic analysis of multiterminal VSC-HVDC grids for offshore wind farms’, *IEEE Trans. Power Deliv.*, 2011, 26, (4), pp. 2476–2485.

[25] Chaudhuri, N., Majumder, R., Chaudhuri, B., et al.: ‘Stability analysis of VSC MTDC grids connected to multimachine AC systems’, *IEEE Trans. Power Deliv.*, 2011, 26, (4), pp. 2774–2784

[26] J. Beerten, S. D'Arco and J. A. Suul, "Frequency-dependent cable modelling for small-signal stability analysis of VSC-HVDC systems," *IET Generation, Transmission & Distribution*, vol. 10, no. 6, pp. 1370-1381, 4 21 2016.

[27] C. Gavriluta, I. Candela, A. Luna, A. Gomez-Exposito and P. Rodriguez, "Hierarchical Control of HV-MTDC Systems With Droop-Based Primary and OPF-Based Secondary," *IEEE Transactions on Smart Grid*, vol. 6, no. 3, pp. 1502-1510, May 2015.

[28] G. Pinares and M. Bongiorno, "Modeling and Analysis of VSC-Based HVDC Systems for DC Network Stability Studies," *IEEE Transactions on Power Delivery*, vol. 31, no. 2, pp. 848-856, April 2016.